Engineering Structures 156 (2018) 363–374

Contents lists available at ScienceDirect

Engineering Structures

journal homepage: www.elsevier.com/locate/engstruct

Collapse mechanisms of masonry arches with settled springing

Paolo Zampieri, Flora Faleschini, Mariano Angelo Zanini*, Nicolò Simoncello

Department of Civil, Environmental and Architectural Engineering, ICEA, University of Padova, Italy

ARTICLE INFO

Keywords:
Masonry arch
Limit analysis
Springing settlement
Collapse mechanism
Thrust line analysis
Cracking hinges

ABSTRACT

Over last centuries, masonry arch has been one of the most used basic structural systems in buildings and infrastructures. One of the most interesting current issues relates safety assessment of existing built heritage, which is often subject to deterioration phenomena. For such reasons, this work aims at analyzing the applicability of classical limit analysis for investigating the safety of masonry arches subject to springing settlements. An extensive parametric analysis is performed considering different geometrical configurations and settlement directions. Then, analytical predictions are compared with results from experimental tests and *FEM* numerical analyses. Such results confirm the reliability of limit analysis when dealing with the safety assessment of settled masonry arches.

1. Introduction

Masonry arch is a structural and architectural system widely diffused in many existing structures, particularly in monumental buildings and bridges. Indeed, during the past centuries, it was often adopted due to its geometrical configuration and ability to carry high values of gravity loads. Compressive stresses arising in the arch elements have lower magnitude than masonry mechanical strength, thus contributing to the widespread diffusion of this system in the past.

In spite of the large diffusion of masonry arch as a structural element, not all the aspects related to its structural behavior are completely known. This reason, together with the increasing interest in the management of existing structures, represents the main cause why the study of masonry arch mechanics is still contemporary. Accordingly, during the last decades many research works studied masonry arch dynamic behavior [1,2], seismic response [3–15], arch-infill interaction [16–18], safety level variation with load values increase [19–26] and retrofit techniques [27–31]. Additionally, many other works focused on developing innovative methods for limit analysis [32–36], numerical analysis [37–53], thrust line analysis [44–50] and reliability-based assessment of some parameters affecting the structural response of the arches [51–56].

However, the effect of external settlement on the structural behavior of masonry arches is not explored in detail yet [57]. Few studies in literature focused on this topic: some of them used limit analysis to assess the influence of settlements at the springing on the structural response of circular [58–61] or pointed arches [62]. In this context, this research work aims to provide a contribution about the knowledge of collapse mechanics occurring in circular masonry arches without keystone, due to settlements at the springing, developed along a generic direction α.

Four main collapse mechanisms can be obtained due to the displacement of one or both supports, as shown in Fig. 1. Mechanism I is symmetric, and it occurs when both the supports are subject to horizontal displacement. Indeed, when the support reaction in the horizontal direction cannot increase to balance the displacement anymore, under virtual displacements, a symmetric three-hinges arch is formed. Hence, this mechanism results in the classical isostatic configuration with three internal hinges (A, B, C), which was studied in detail in literature [58–61]. Particularly, Oschendorf [59,60] highlighted how the internal hinges position and the horizontal thrust generated by the arch change with the geometry of the element (radius R, thickness t, angle of embrace β), through a thrust line analysis. Coccia et al. [61] continued the work of Oschendorf, proposing an innovative method based on applying the kinematic theorem on the deformed configuration of the arch. They demonstrated that the position of the internal hinges changes with the increase of the horizontal displacement at the supports.

Less attention is paid in literature regarding other mechanisms that may occur due to the settlement of arch supports. Accordingly, in this research work, mechanisms II, III and IV are studied in detail. These configurations are due, respectively, to a horizontal, an inclined and a vertical settlement, applied to a single support of the arch.

Principle of Virtual Work (*PVW*) is applied in the undeformed configuration, together with a thrust line analysis, to study the above mechanisms, and univocally find the location of the hinges, as done also

* Corresponding author.
E-mail address: marianoangelo.zanini@dicea.unipd.it (M.A. Zanini).

https://doi.org/10.1016/j.engstruct.2017.11.048
Received 16 May 2017; Received in revised form 17 November 2017; Accepted 20 November 2017

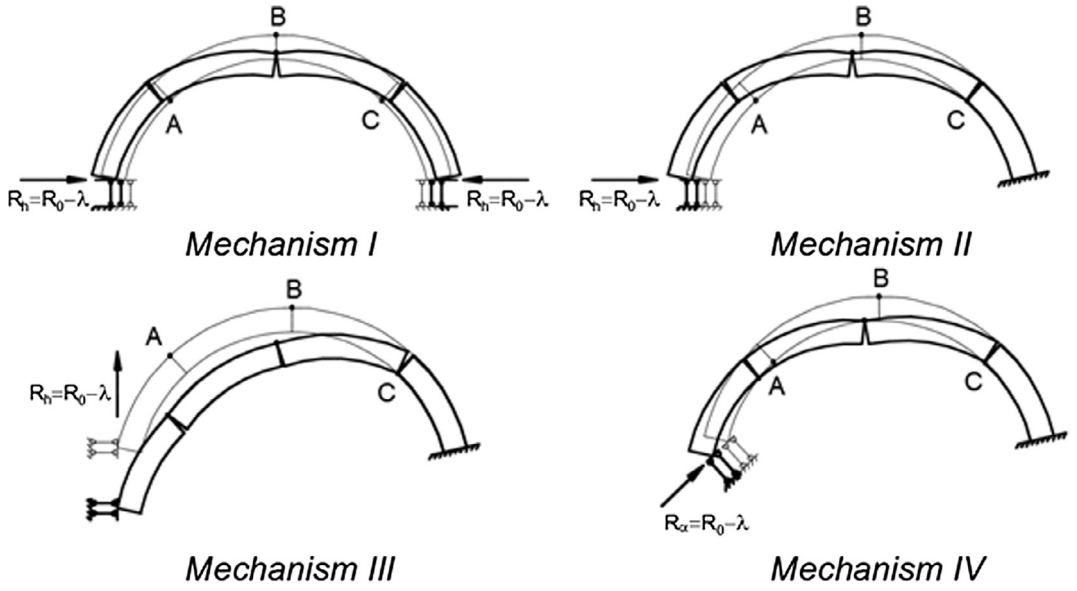

Fig. 1. Main masonry arch collapse mechanisms due to supports settlement.

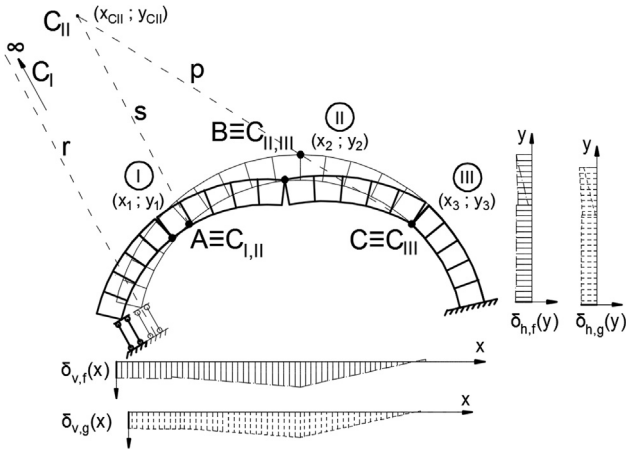

Fig. 2. Virtual displacement diagrams of masonry arch collapse mechanism.

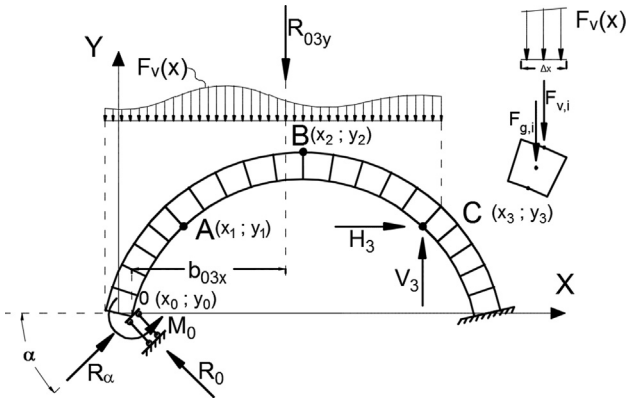

Fig. 3. Scheme of the forces and reactions applied at the masonry arch.

in [61]. This procedure is used here for the first time to study mechanisms II, III and IV. The combination of these approaches allows identifying the statically admissible mechanism between all the kinematics admissible ones, derived through the application of the kinematic theorem. Results obtained in this work provide the hinges position varying the angle of settlement direction α, arch geometry, and the support reaction in the direction of the external settlement R_α. Then,

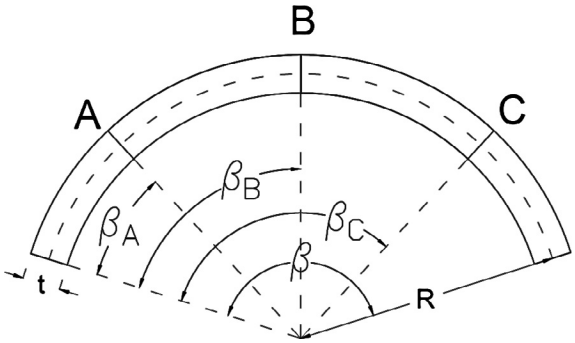

Fig. 4. Geometrical parameters considered in parametrical analysis.

Table 1
Geometrical parameters adopted.

	t/R				
$\beta = 180°$	0.135	0.15125	0.1675	0.18375	0.2
$\beta = 155°$	0.07	0.1025	0.135	0.1675	0.2
$\beta = 125°$	0.03	0.0725	0.115	0.1575	0.2
$\beta = 90°$	0.015	0.04875	0.0825	0.11625	0.15
$\beta = 45°$	0.015	0.01875	0.0225	0.02625	0.03

two experimental tests are carried out on two masonry arches with mortar joints. The arches have the same geometry but the external settlement is different: in one case, a vertical displacement was imposed to a single support; in the other, the displacement was inclined with $\alpha = 45°$. Lastly, experimental results are compared with the analytical ones obtained with limit analysis, and also to numerical ones derived with a finite element model.

2. Limit analysis of masonry arch subject to displacement at the supports

Limit analysis is the most used method to assess the ultimate capacity and collapse mechanism configuration of a masonry arch. This approach, initially proposed by Heyman [63–64], is based on four fundamental hypotheses: elastic strains are considered negligible; infinite shear strength; masonry with no tensile strength; masonry with infinite compressive strength. This last assumption can be removed

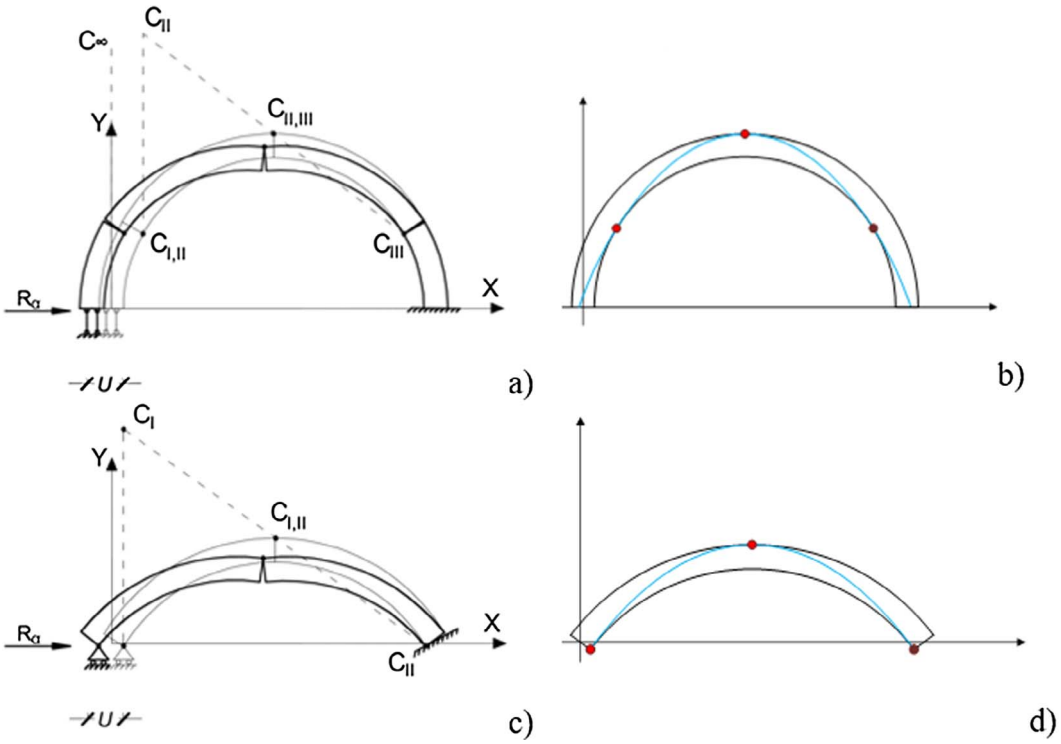

Fig. 5. Collapse configurations (a, c) and lines of pressures (b, d) – Mechanism II.

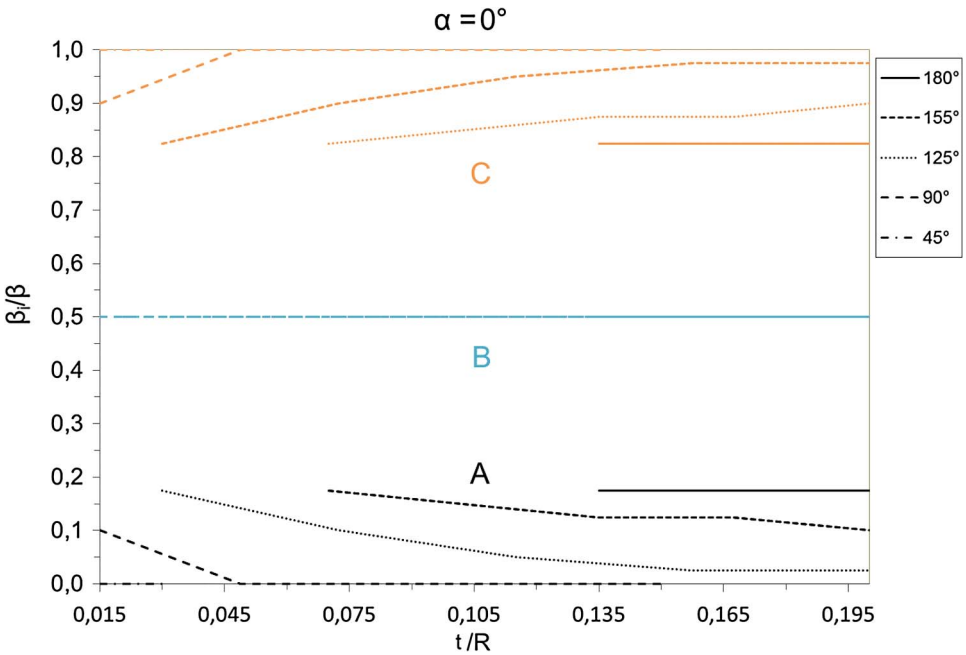

Fig. 6. Hinges position (β_i/β) varying the angle of embrace and t/R ratio values – Mechanism II.

taking into account the limited compressive strength of the material, through re-allocating the hinge position at the center of the idealized plastic deformation region [14,25].

According to Heyman hypotheses, the ultimate load is achieved when the line of pressure, which is completely inside the masonry arch, becomes tangent at the arch boundary in enough points. These points are considered as the internal crack hinges.

Kinematic theorem is used here to calculate the value of the support reaction R_α that triggers the mechanism. Then, it is possible to draw the line of pressure, with the aim to verify if it lays inside the arch, and if it is tangent to the boundary of the arch in the crack hinges locations, thus ensuring that is statically admissible (i.e. using the static theorem). If the mechanism is both statically and kinematically admissible, then the value of R_α calculated with the *PVW* is effectively the support reaction, in the direction of the external settlement.

Taking as reference the mechanism shown in Fig. 2, the general expression of the *PVW* can be written as:

$$\int F_v(x)\cdot\delta v_F(x)dx + \int g\cdot\delta v_g(x)dx + R_\alpha\cdot\delta_s(x_0,y_0) = \int \sigma\cdot\varepsilon dV \qquad (1)$$

where the left side is the external work, and the internal work is reported at the right side of the equation. Particularly, considering Fig. 3 for the definition of the applied forces:

$F_v(x)$, g, R_α are respectively the external vertical forces applied to

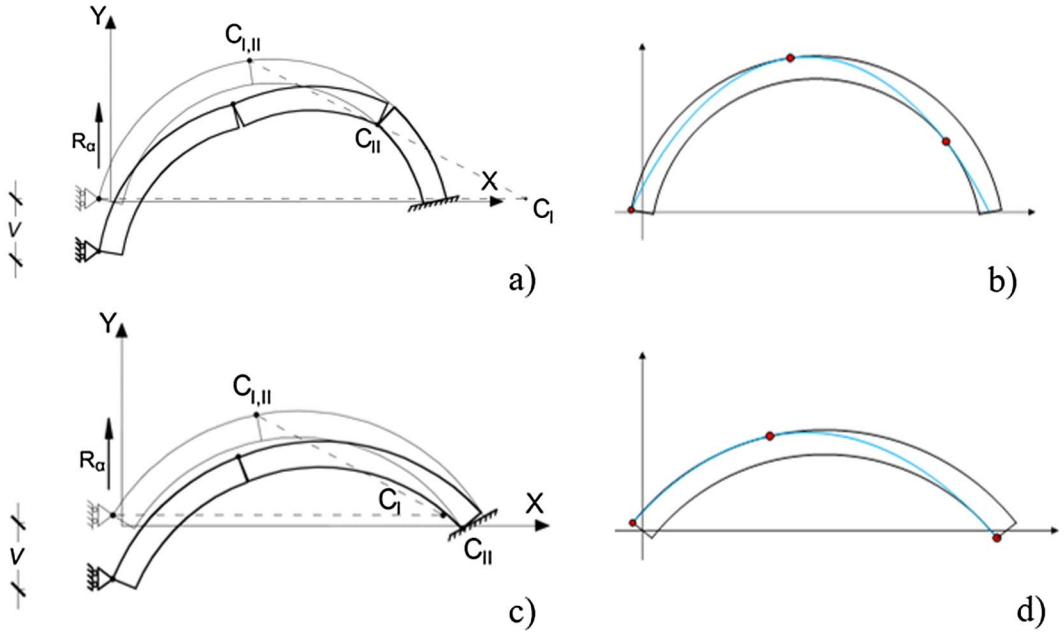

Fig. 7. Collapse configurations (a, c) and lines of pressures (b, d) – Mechanism III.

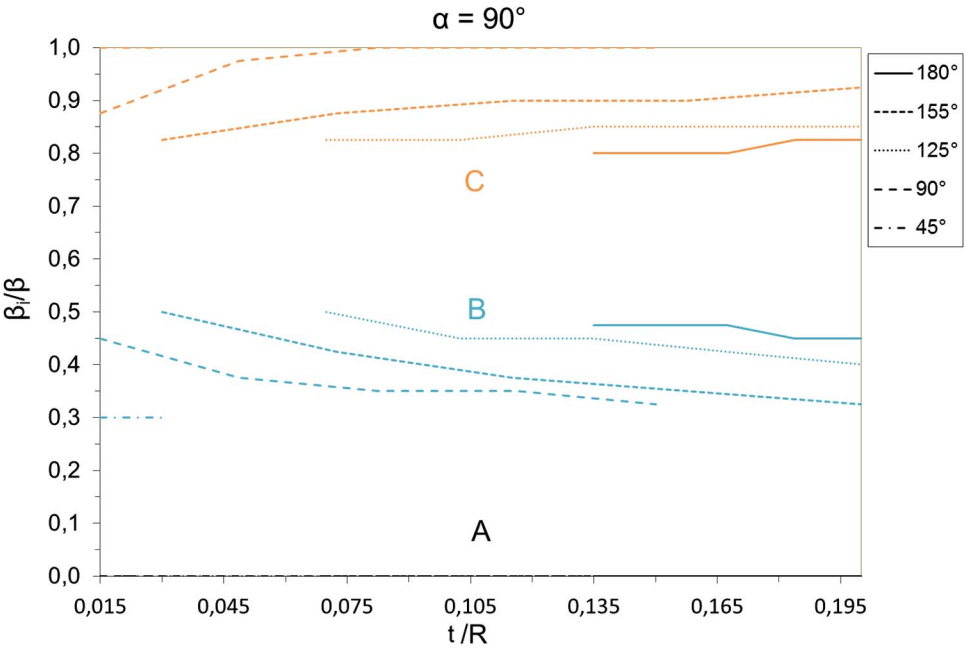

Fig. 8. Hinges position (β_i/β) varying the angle of embrace and t/R ratio values – Mechanism III.

the arch, gravity forces, and the support reaction in the direction of the external settlement;

$\delta v_F(x)$, $\delta v_g(x)$, $\delta_s(x_0, y_0)$ are respectively vertical virtual displacement due to $F_v(x)$, g, and virtual displacement due to R_α in the direction of the external settlement.

Virtual displacement field is defined with the hypothesis of small displacement, and assuming hinges coordinates A (x_1, y_1), B (x_2, y_2), C (x_3, y_3), which separate the arch in three rigid blocks, as shown in Fig. 2. Fig. 2 shows also the position of the centers of rotation, both principal (C_I, C_{II}, C_{III}) and relative between two successive blocks ($C_{I,II}$ and $C_{II,III}$). The coordinates of these last two relative centers coincide with the ones of the crack hinges A and B. C_I belongs to the line r, whereas C_{II} is located at the intersection between line s and p: s is parallel to r and p passes from both $C_{II,III}$ and C_{III}. Hence, the coordinates of C_{II} are:

$$x_{C_{II}} = \frac{t_2 - t_1}{m_1 - m_2}; \qquad y_{C_{II}} = x_{C_{II}} m_2 + t_2 \tag{2}$$

where m_2 and t_2 are the slope and intercept of line p; m_1 and t_1 are the slope and intercept of line s, and they can be expressed as:

$$m_2 = \frac{x_3 - x_2}{y_3 - y_2} \qquad t_2 = x_2 m_2 + y_2 \tag{3}$$

$$m_1 = \tan\left[\left(\frac{\pi}{2}\right) - \alpha\right] \qquad t_1 = -x_1 m_1 + y_1 \tag{4}$$

Then it is possible to express each component of the virtual displacement field, recalling that the rotation of the second rigid block is related with the rotation of the first, according to:

$$\varphi_2 = \varphi_1 \frac{x_2 - x_{C_{II}}}{x_3 - x_2} \tag{5}$$

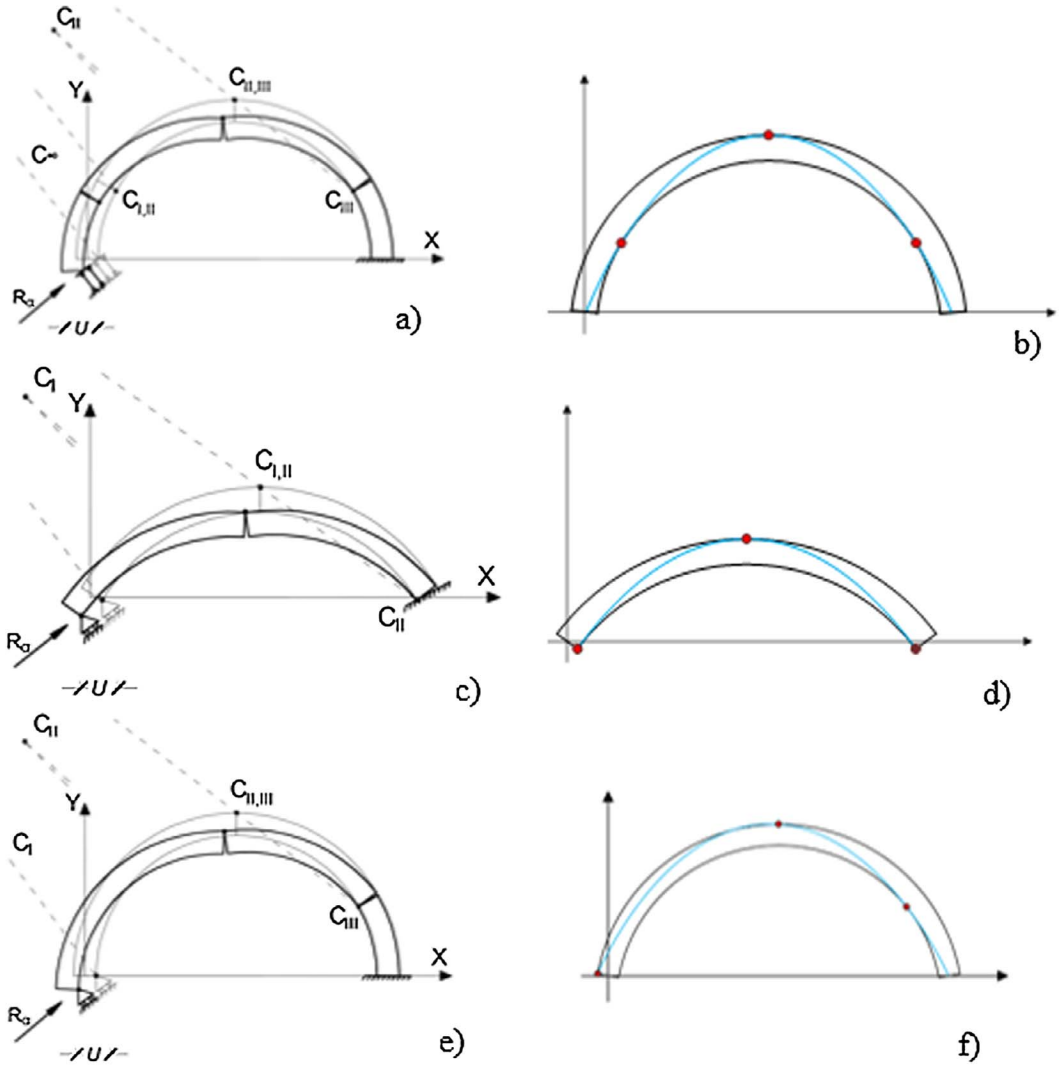

Fig. 9. Collapse configurations (a, c, e) and lines of pressures (b, d, f) – Mechanism IV.

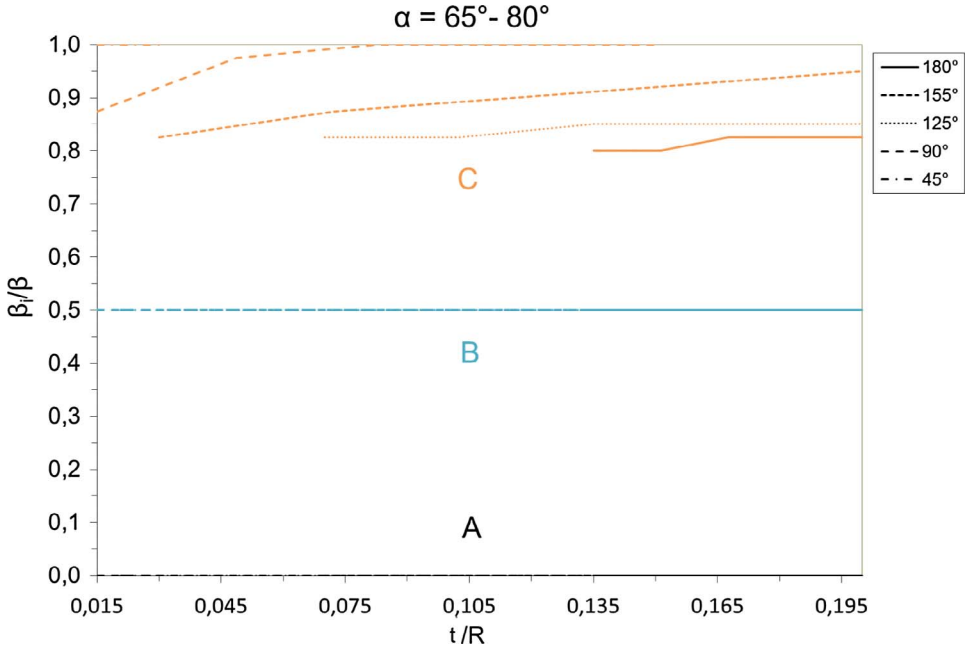

Fig. 10. Hinges position (β_i/β) varying the angle of embrace and t/R ratio values – Mechanism IV, α = 65–80°.

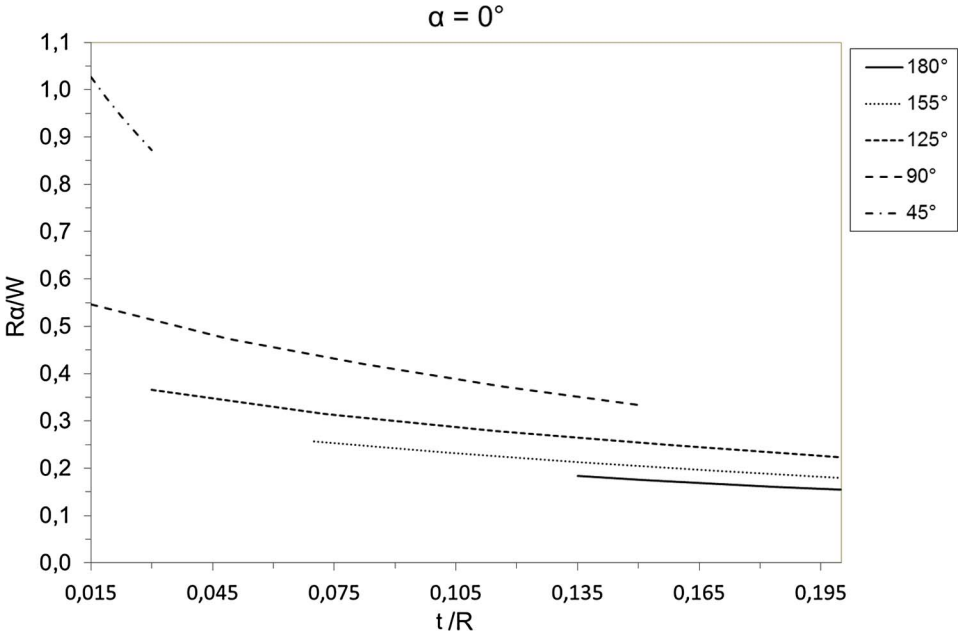

Fig. 11. Collapse thrust varying the angle of embrace and t/R ratio – Mechanism II.

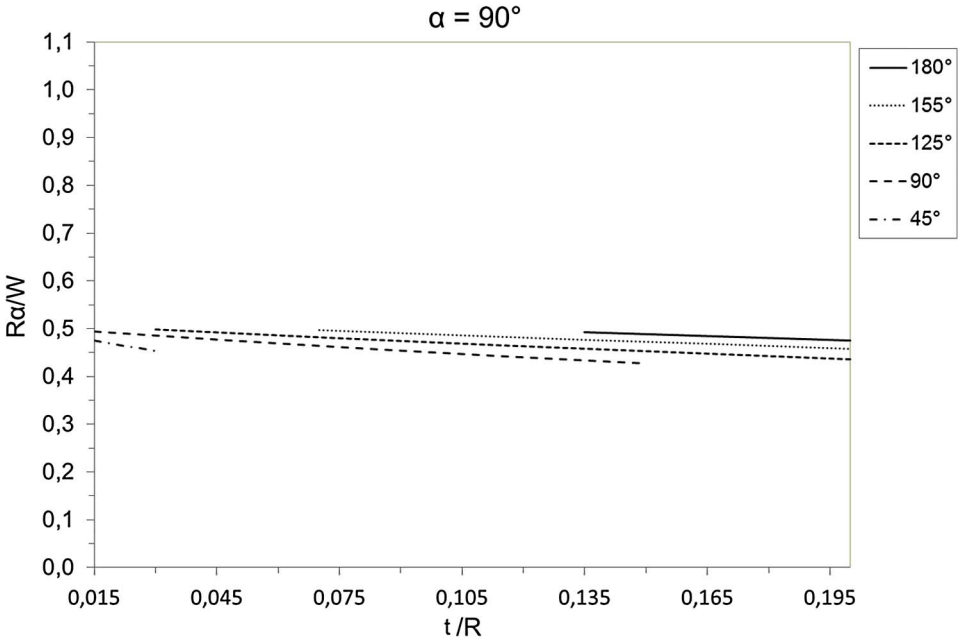

Fig. 12. Collapse thrust varying the angle of embrace and t/R ratio – Mechanism III.

Hence, the virtual horizontal and vertical displacement of block I can be obtained as:

$$\delta_{h,1}(y) = (y_1 - y_{C_{II}})\varphi_1 = cost \quad \delta_{v,1}(x) = -(x_1 - x_{C_{II}})\varphi_1 = cost \tag{6}$$

In the same manner, the virtual horizontal and vertical displacement of block II can be obtained as:

$$\delta_{h,2}(y) = (y - y_{C_{II}})\varphi_1 \qquad \delta_{v,2}(x) = -(x - x_{C_{II}})\varphi_1 \tag{7}$$

Lastly, the virtual horizontal and vertical displacement of block III are:

$$\delta_{h,3}(y) = (y - y_3)\varphi_2 \qquad \delta_{v,3}(x) = -(x - x_3)\varphi_2 \tag{8}$$

Looking at the right side of Eq. (1), the internal work can be assumed null according to the hypothesis of negligible elastic strains. Lastly, if we consider the arch as a discrete body made with distinct rigid elements (e.g. a defined number of voussoirs), the continuous form of Eq. (1) becomes:

$$L_e = \sum_{i=1}^{n} F_{v,i} \cdot \delta v_{F,i} + \sum_{i=1}^{n} g_i \cdot \delta v_{g,i} + R_\alpha \cdot \delta_s(x_0, y_0) = 0 \tag{9}$$

where:

$F_{v,i}$, g_i are respectively the external vertical forces and the gravity forces applied to each i-rigid block of the arch;

$\delta v_F, i$, $\delta v_{g,i}$ are respectively vertical virtual displacement due to F_v, i and g_i applied to each i-rigid block of the arch.

From Eq. (9), the value of the support reaction R_α can be obtained, as follows:

$$R_\alpha = \frac{\sum_{i=1}^{n} F_{v,i} \cdot \delta v_{F,i} + \sum_{i=1}^{n} g_i \cdot \delta v_{g,i}}{\delta_s(x_0, y_0)} \tag{10}$$

At this step, all the necessary elements to draw the line of pressures are known: it can be easily obtained calculating the internal forces between each interface of the discrete blocks constituting the arch.

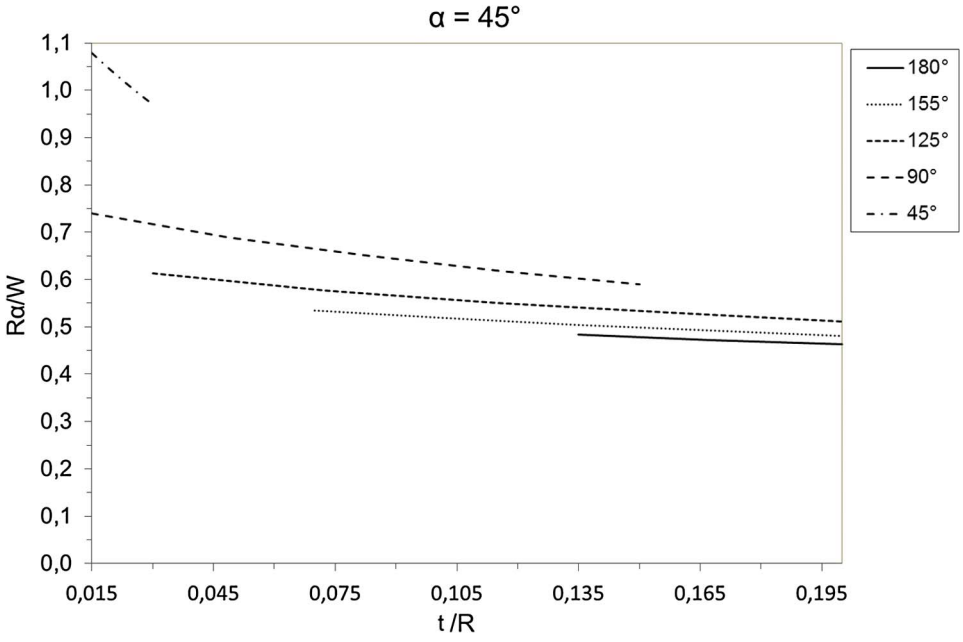

Fig. 13. Collapse thrust varying the angle of embrace and t/R ratio – Mechanism IV ($\alpha = 45^{\circ}$).

These forces are obtained using the equilibrium equations, once the constraint reactions are known at the collapse, calculated as it follows:

$$[Q]\{\mathbf{q}\}^T = \{\mathbf{R}\} \tag{11}$$

where [Q] is the static matrix, which components are:

$$[Q] = \begin{bmatrix} 1 & 0 & 1 & 0 \\ -\tan\alpha & 0 & 0 & 1 \\ 0 & -1 & (x_0 - x_3) & (y_3 - y_0) \\ 0 & 0 & (x_2 - x_3) & (y_3 - y_2) \end{bmatrix} \tag{12}$$

{**R**} is the vector containing the constraint reactions, having the following components:

$$\{\mathbf{R}\}^T = \{V_0\, M_0\, V_3\, H_3\}^T \tag{13}$$

and lastly {**q**}T is known, as its components are:

$$\{\mathbf{q}\}^T = \{R_{03y} - R_{vv} - R_{vh} - R_{03y} b_{03x} - R_{23y} b_{23x}\}^T \tag{14}$$

In the expression from Eq. (11) to Eq. (14), the following notations are used:

V_0 is the vertical component of the constraint reaction R_0, from which it is possible to calculate also the horizontal component of R_0, $H_0 = V_0 \tan \alpha$;

M_0 is the resisting moment at the node with coordinates (x_0, y_0);

V_3 and H_3 are respectively the vertical and horizontal component of the constraint reaction at the hinge C (x_3, y_3);

R_{vv} and R_{vh} are respectively the vertical and horizontal component of the force R_{α};

R_{03y} is the resultant of the external forces applied to the arch between (x_0, y_0) and (x_3, y_3), and b_{03x} is the distance between (x_0, y_0) and the point of application of R_{03y};

R_{23y} is the resultant of the external forces applied to the arch between (x_2, y_2) and (x_3, y_3), and b_{03x} is the distance between (x_2, y_2) and the point of application of R_{23y}.

If both the static and the kinematic theorems are satisfied, the solution can be considered correct. This means that, according to the line of pressure derived in this manner, if it lays in the arch profile and it is tangent to the boundary at the hinges location (i.e. in A, B and C points), then the solution is correct. The solution can be obtained iteratively, continuously updating the hinges position until satisfying static theorem, as described in Zampieri et al. [13].

3. Influence of arch geometry on hinges position at the collapse

Settlements (horizontal, vertical or inclined) at the support of an arch are responsible for the formation of three crack hinges (A, B and C), which transform the structure in a mechanism, according to Heyman hypotheses. However, their position depends on the arch geometry. Accordingly, a parametric analysis is performed here to assess the influence of geometrical parameters on the location of such points.

To perform the analysis for each mechanism (II, III and IV, according to Fig. 1), only dead load is considered due to the self-weight of masonry (here assumed equal to 18 kN/m^3). Then, five values of the angle of embrace of the arch β are chosen, and for each, five values of thickness-to-internal radius t/R ratio are considered (Fig. 4), as shown in Table 1. Lastly, the direction of the external applied settlement is varied between 0 and 90°, with increasing steps of 2°.

Concerning the results obtained for mechanism II, it is worth noting that the hinges are located symmetrically with respect to the key-stone, for each collapse configuration that may arise varying the above parameters. Fig. 5 shows two possible configurations (a, c), for two cases with different values of β, and their respective lines of pressure (b, d). In both cases, the hinge B is located at the extrados of the arch, thus the dimensionless angle of embrace β_B/β becomes 0.5. Conversely, the values of the dimensionless angle of embrace β_B/β of the other two hinges vary depending on the angle β and on the t/R ratio, as shown in Fig. 6.

Particularly, Fig. 5a shows the collapse configuration of semi-circular arches: A and C hinges are located, respectively, at an angular distance equal to $\beta_A/\beta = 0.2$ e a $\beta_C/\beta = 0.8$. Then, looking at Fig. 6, it is worth to note that the t/R ratio influences the hinges location, too: with its increase, the hinges move close to the support.

Now, let us consider mechanism III: the main difference with the previous case is due to the absence of symmetry in the hinges formation. Indeed, the hinge B is not located anymore at the keystone of the arch, as it is shown in Fig. 7. On the contrary, two successive hinges arise at the extrados (A and B), whereas hinge C is located at the intrados. This configuration represents an uncommon situation in masonry arch behavior: typically, two successive hinges are located alternatively at the intrados and extrados, as it occurs due to a concentrated load at the mid-span [23] or due to seismic action [1]. Considering the segmental arch of Fig. 7c, it is worth noting that the

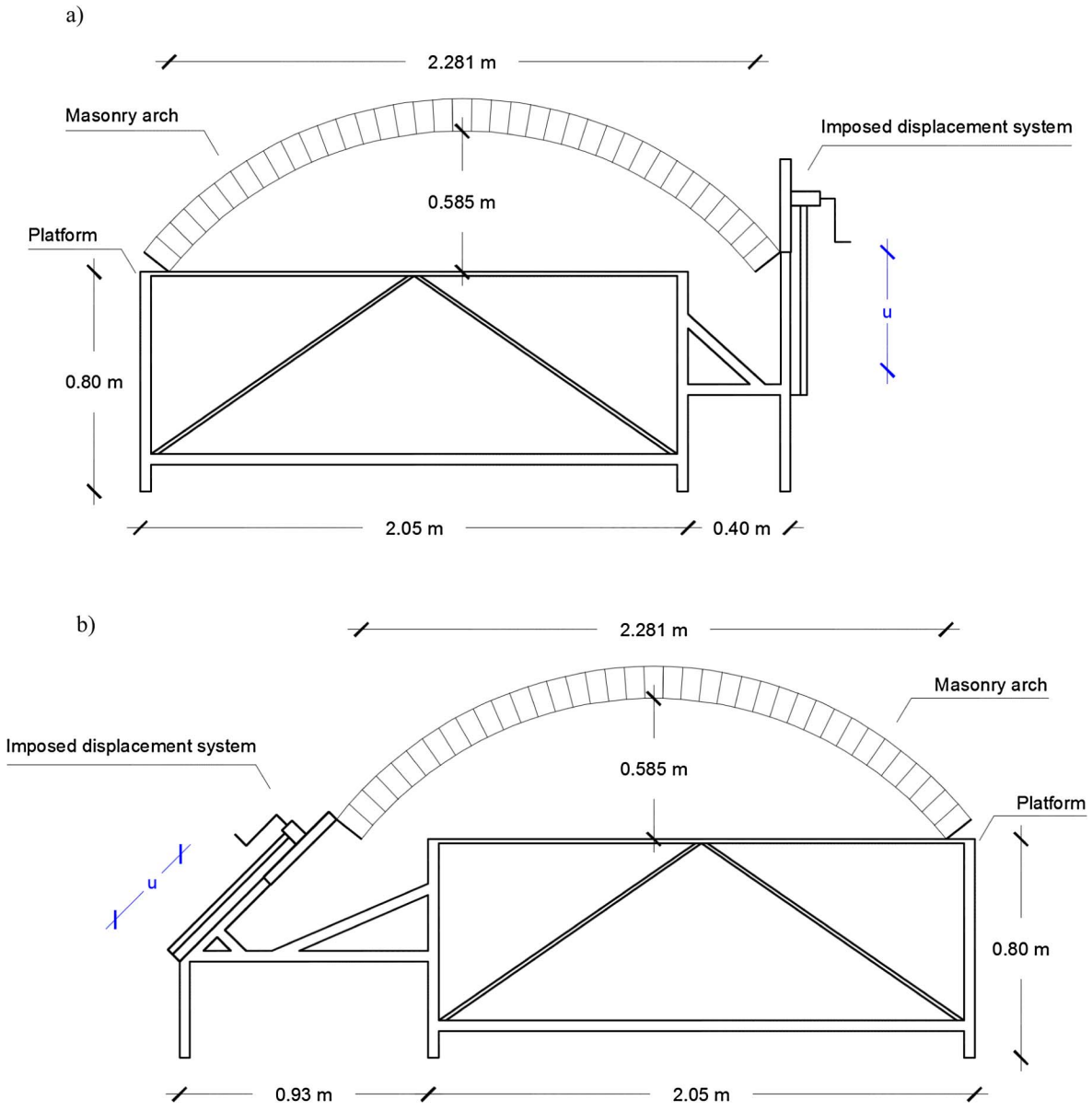

Fig. 14. Specimens geometry and test layout: (a) $\alpha = 90^{\circ}$; (b) $\alpha = 45^{\circ}$.

Table 2
Mortar and brick main properties.

Element	Density [kg/m^3]	Compressive strength [MPa]	Young modulus [MPa]	Flexurale strength [MPa]
Mortar (M5 Compressive Strength Class)	1500	> 5	8000	> 2
Clay Brick (250 × 120 × 55 mm^3)	1454	22	27,000	–

line of pressures (shown in Fig. 7d) between point A and B is almost tangent to the extrados line of the arch.

Fig. 8 shows that, despite the geometry of the arch, the hinge A is always located at the springing; instead, the hinge C is located at the springing only for arches with $\beta = 45^{\circ}$ and $\beta = 90^{\circ}$ with t/R ratio > 0.08.

The last analyzed case concerns when settlement is applied along the generic direction α (mechanism IV). In this case, the results of the parametric analysis highlight how the configuration of the collapse mechanism depends highly on the angle α. Three macro-ranges were selected to discuss the results: α value below 48°; between 66° and 80°; between 48° and 66° and higher than 80°.

In the first case, the position of the hinges is exactly the same than in Mechanism II, with a horizontal settlement. In this range, the plot which identify the hinges position varying the angle of embrace and t/R ratio values is the same than Fig. 6. The collapse configuration is shown in Fig. 9a, which is influenced by the dominant component of horizontal displacement on the overall external settlement applied at one springing.

The second case applies when the values of the angle β is between 66° and 80°. In this range, the hinge A moves from the intrados to the extrados of the arch, whereas the dimensionless value of the angle β_B is always equal to 1 in all the analyzed cases. Lastly, the position of the hinge C depends on the t/R ratio and angle of embrace, as shown for instance in Fig. 9e. The hinges position is instead represented in Fig. 10.

The last range of angle α values represents a set of situations where the location of hinges seems randomly dependent on the analyzed variables. Indeed, in these cases, both the configuration of extrados-

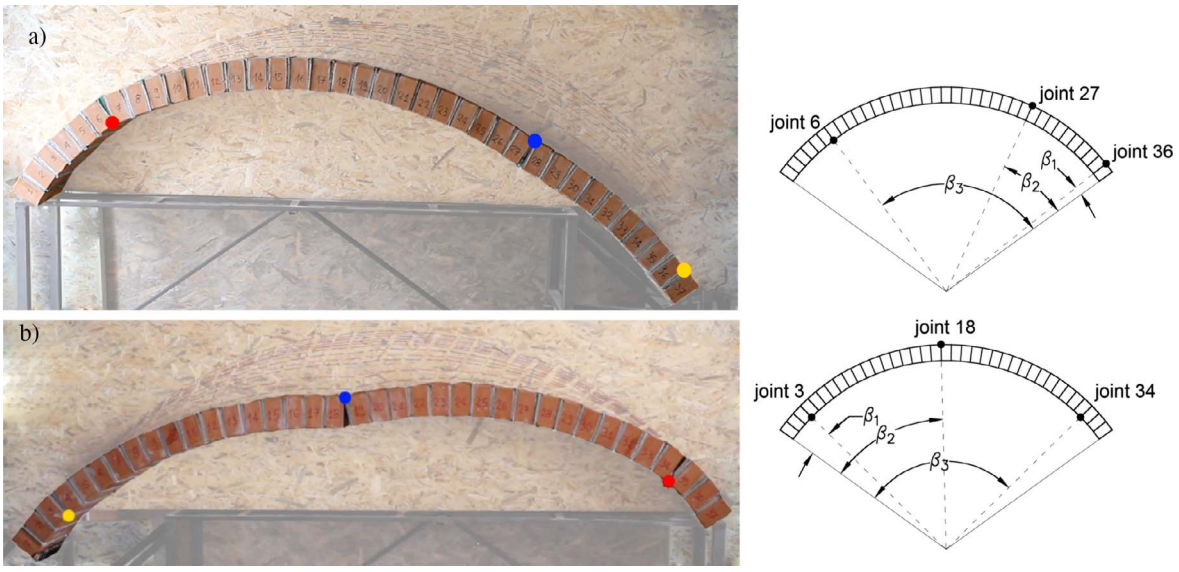

Fig. 15. Experimental collapse configuration: (a) $\alpha = 90^{\circ}$; (b) $\alpha = 45^{\circ}$.

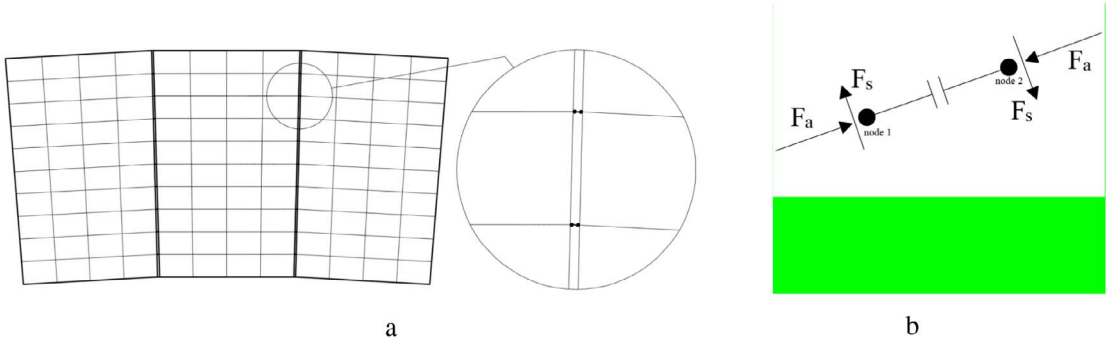

Fig. 16. (a) Mesh of each voussoir with 2D quadrangular elements, and *point-contact* elements for mortar joints modeling. (b) *Point-contact* scheme.

Table 3
Material properties in the finite element model.

Masonry bricks			Mortar joints		
E [MPa]	ν	ρ [kg/m^3]	k_a [N/mm]	k_s [N/mm]	μ
132,000	0.25	1390	$1.2 * 10^6$	10^{10}	0.6

intrados-extrados hinges and intrados-intrados-extrados hinges may occur.

4. Influence of arch geometry on collapse thrust

Due to the applied settlement, a loss of the horizontal reaction is observed at the settled support. Hence, similarly, the value of the thrust changes from R_0 to R_α at the collapse, as obtained according to the static and kinematic theorems application, with Eq. (10).

Here, collapse thrust is analyzed for the three mechanisms discussed above, namely mechanism II, III and IV, the last assuming an angle $\alpha = 45^{\circ}$. For each mechanism, the dimensionless ratio R_α/W between the thrust (along the displacement direction) and the self-weight of the arch is calculated, for varying values of t/R and β, as done in Section 3. Results are summarized in Figs. 11–13.

Figure 11 shows that the reduction of the angle β has a strong influence on the value of the thrust, when a horizontal displacement is applied at one support. The value of R_α changes of about 80% of W, if the angle of embrace changes from 45° to 180°.

Fig. 12 refers instead to a vertical displacement applied at one support: in this case, the value of R_α does not change significantly in the analyzed range of geometrical properties. Indeed, its value ranges between 40% and 55% of the self-weight of the arch, respectively in case of $\beta = 180^{\circ}$ and 45°.

Lastly, Fig. 13 refers to the case of an inclined displacement with an angle α of 45°. Here, the variation of the thrust value is significant too, such as for $\alpha = 0^{\circ}$, both varying the angle of embrace and the t/R ratio. Indeed, R_α assumes values between 50% and 110% of W.

5. Experimental tests

Two experimental tests are carried out on real scale arches with the same geometry, and subject to settlement with two directions, aiming to compare these results with the ones obtained through limit analysis. The geometry of the arches and the test layout are shown in Fig. 14. According to their dimensions, the arches can be assimilated to segmental arches, realized with a single raw of 37 voussoirs. Main material properties of bricks and mortar are listed in Table 2. The displacement is applied with a mechanical system having a precision of ± 2 mm. Concerning the test layout, the arch is placed onto a braced truss which can be considered infinitely stiff with respect to the applied displacement.

Concerning the results, Fig. 15a shows the experimental collapse mechanism obtained applying a vertical settlement at the support: as obtained from the limit analysis results too, the experimental evidence proves that an asymmetric configuration of hinges position occurs. The main feature of this configuration is that two following hinges are located at the extrados, and they are placed at mortar joints 27 and 36, as

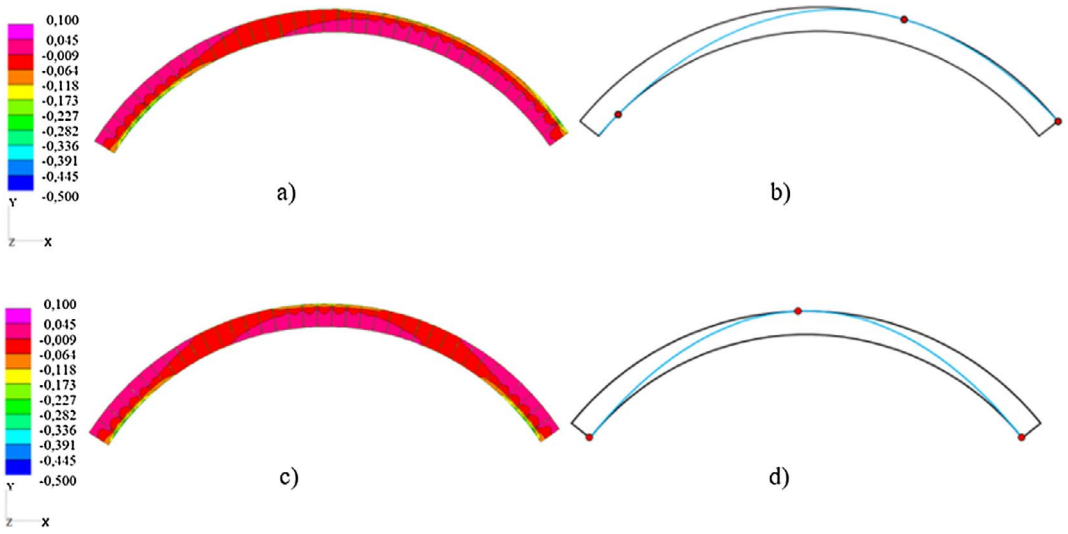

Fig. 17. (a) Contour of principal compressive stress $\alpha = 90°$; (b) Thrust line $\alpha = 90°$; (c) Contour of principal compressive stress $\alpha = 45°$; (d) Thrust line $\alpha = 45°$.

Table 4
Comparison between experimental test (ET), limit analysis (LA) and finite element analysis (FEA) results.

α	90°			45°		
Analysis method	*ET*	*LA*	*FEA*	*ET*	*LA*	*FEA*
β_A/β	3	1	2	6	3	4
β_B/β	18	18	19	27	24	23
β_C/β	34	36	36	35	35	35
R_α [kN]	–	0.6014	0.6151	–	0.8673	0.9162

shown in Fig. 15a. Fig. 15b illustrates instead how mechanism IV is developed, with $\alpha = 45°$. As highlighted in Section 3, in this case the value of the angle at which the displacement is applied belongs to the first range of values identified (less than 48°). Hence, the mechanism is symmetric, with the classical configuration of intrados-extrados-intrados three-hinges arch.

6. Finite element modeling

A two-dimensional finite element non-linear analysis is then carried out to compare both the experimental and limit analysis results. The mesh is realized modeling each voussoir with 40 elements (Fig. 16a); joints are modeled as 1D contact elements (*point-contact*) (Fig. 16b), and a linear elastic model is used for the bricks masonry material properties, which are listed in Table 3. The 2D finite element used for the numerical analyses is a 4-node quadrilateral isoparametric plate element (Quad4) with constant thickness, four Gauss integration points and linear shape functions.

Masonry arch specimens used in the experimental campaign are characterized by no-tensile strength between masonry blocks, due to the presence of a plate made with plexiglass, located in the middle of each mortar joint. In these conditions, the interface between each blocks transfers only compressive and shear stresses. Hence, the choice of using point-contact (a non-linear 1D element) for the joints well represents the experimental contact behavior between the blocks, with unilateral friction [65]. Alternative approaches can be followed to model mortar joints, e.g. to take into account tensile strength of mortars in dry joints [10].

Point-contact elements are characterized by a negative value of the strain (at maximum, equal to 0), which is defined according to Eq. (15):

$$0 > \frac{\Delta L}{L_0} > \varepsilon_p \tag{15}$$

where ε_p is the maximum allowed strain, limited by the mortar joint thickness. The axial force F_a acting in the *point-contact* element is proportional to the length variation of the element ΔL, and to its axial stiffness k_a, as shown in Eq. (16):

$$F_a = k_a \Delta L \tag{16}$$

Instead the lateral force value assumes a constant value if it exceeds

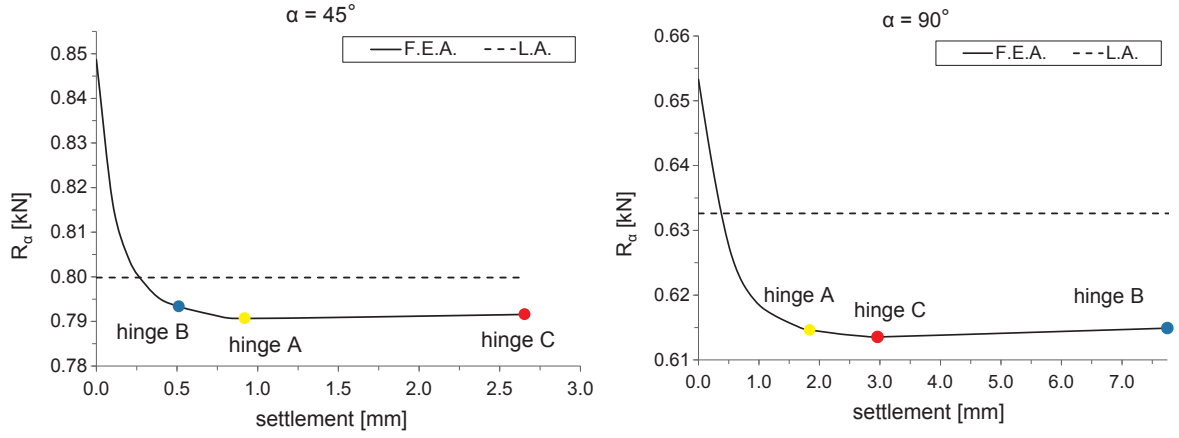

Fig. 18. Thrust-displacement curves of settled springing: (a) $\alpha = 90°$; (b) $\alpha = 45°$.

the static friction force ($\mu \cdot F_a$), otherwise it is proportional to the tangent stiffness of the element k_s:

$$F_s = \mu F_a \quad \text{for}] \quad k_s \Delta T \geqslant \mu F_a \tag{17}$$

$$F_s = k_s \Delta T \quad \text{for} \quad k_s \Delta T < \mu F_a \tag{18}$$

where ΔT is the relative lateral displacement between two external nodes of the contact elements. The other parameters are instead defined in Table 3, together with bricks masonry properties.

Two non-linear analyses are performed: in the former, a vertical displacement is applied to one springing; in the latter, the applied displacement is inclined by an angle $\alpha = 45^\circ$. The model is able to adequately capture the collapse hinges formation through the discretization of the *point-contact* elements. Particularly, Fig. 17a and c show the contour of the principal compressive stresses in the arch at the instant when the third cracking hinge is formed. The hinge section can be easily identified because one only *point-contact* is still active, at the compressed boundary. In these sections, the most stressed fibers are subject to a compressive stress of 0.5 MPa. This value is sensibly less than the compressive strength of the masonry. This outcome is confirmed also from the experimental evidences, that do not reveal any crushing phenomena, thus justifying the assumption of linear elastic properties for the masonry.

From Fig. 17a and c it is also possible to derive the thrust line configurations, shown in Fig. 17b and d, which substantially are the same than the one obtained with the limit analysis.

7. Discussion of the results

The collapse mechanisms analyzed in this work were not fully investigated in literature, and hence this research aims to comprehensively investigate these situations, through different approaches. Hence, the first objective is to clearly identify the collapse configurations according to the direction of the external settlement applied to one support of the arch, and to its geometry, through limit analysis, experimental tests and a numerical approach. All the proposed methods provide almost the same results, agreeing for the two analyzed situations, i.e. with vertical and inclined displacement, this last with $\alpha = 45^\circ$. Those methods not only provide the same collapse configuration (i.e. asymmetric mechanism with extrados – extrados – intrados hinges for $\alpha = 90^\circ$; symmetric mechanism with intrados – extrados – intrados hinges for $\alpha = 45^\circ$), but also they localize the position of the hinges almost in the same places. Indeed, Table 4 lists the position of the hinges A, B, C (according to the nomenclature of Fig. 1) at the mortar joints, numbered as in Fig. 15. It is possible to observe that, at maximum, the position provided by limit analysis and FEA differs for one position. Instead, results provided by the experimental tests and the other methods (limit analysis and FEA), differ from three or four positions. Additionally, comparing the values of the thrust R_α obtained by limit analysis and FEA, the error between the two provisions is between 2.27% and 4.89%.

Then, Fig. 18 shows the variation of the thrust with the applied displacement at the springing. It is possible to observe that in both the cases the displacement value which triggers the mechanism is low: particularly, it is equal to 8.5 mm for $\alpha = 90^\circ$ and to 2.7 for $\alpha = 45^\circ$. Additionally, the value of the thrust changes also at low values of the displacement: in the initial condition it assumes a maximum value, then it decreases with the settlement amount, until a minimum over that it is almost stable before the collapse. It is worth to note that when all the three hinges are localized in the arch, the thrust value is not the minimum, but it is slightly higher, due to the geometrical non-linearity. Indeed, with the increase of the applied displacement, also the arch shape changes, thus influencing the value of the horizontal reaction.

8. Conclusions

This paper investigates the mechanics of masonry arches subject to settlement at one support. The analyzed displacements are vertical, horizontal and also inclined by a generic angle α. Three approaches are used to study the problem: limit analysis, experimental tests and finite element non-linear analysis. Particularly, limit analysis allows to obtain, through the use of the static and kinematic theorem, the value of the thrust R_α at the settled support, in the same direction of the displacement application. With this method, it is possible to observe how the possible mechanisms are developed, being in all the cases three-hinges arches, with varying configuration of the cracks hinges. This simplified approach provides solutions that are reasonably comparable to ones obtained with non-linear finite element analysis, and which are also confirmed by experimental evidences. Accordingly, the simplifying hypotheses at the base of limit analysis approach can be consider valid to study these kind of problems, where the collapse is reached under small displacements, as experimentally proved.

Concerning the configuration of the two studied mechanisms, it is worth noting that the direction of the external displacement plays a key-role in defining the location of the hinges. Also the geometrical parameters of the arch significantly affect the collapse configuration.

Appendix A. Supplementary material

Supplementary data associated with this article can be found, in the online version, at http://dx.doi.org/10.1016/j.engstruct.2017.11.048.

References

[1] De Lorenzis L, DeJong M, Ochsendorf J. Failure of masonry arches under impulse base motion. Earthq Eng Struct Dyn 2007;36:2119–36.
[2] Misseri G, Rovero L. Parametric investigation on the dynamic behaviour of masonry pointed arches. Arch Appl Mech 2017;87(3):385–404.
[3] Brandonisio G, Mele E, de Luca A. Limit analysis of masonry circular buttressed arches under horizontal loads. Meccanica 2017:1–19.
[4] Alexakis H, Makris N. Hinging mechanisms of masonry single-nave barrel vaults subjected to lateral and gravity loads. J Struct Eng (United States) 2017;143(6). art. no. 04017026.
[5] Ramaglia G, Lignola GP, Prota A. Collapse analysis of slender masonry barrel vaults. Eng Struct 2016;117:86–100.
[6] Marefat MS, Yazdani M, Jafari M. Seismic assessment of small to medium spans plain concrete arch bridges. Eur J Environ Civil Eng 2017. http://dx.doi.org/10.1080/19648189.2017.1320589.
[7] Cavalagli N, Gusella V, Severini L. Lateral loads carrying capacity and minimum thickness of circular and pointed masonry arches. Int J Mech Sci 2016;115–116:645–56.
[8] De Santis S, de Felice G. A fibre beam based approach for the evaluation of the seismic capacity of masonry arches. Earthquake Eng Struct Dyn 2014;43:1661–81.
[9] Sayin E. Nonlinear seismic response of a masonry arch bridge. Earthq Struct 2016;10(2):483–94. http://dx.doi.org/10.12989/eas.2016.10.2.483.
[10] Gaetani A, Lourenço PB, Monti G, Moroni M. Shaking table tests and numerical analyses on a scaled dry-joint arch undergoing windowed sine pulses. Bull Earthq Eng 2017;15(11):4939–61.
[11] Zampieri P, Zanini MA, Modena C. Simplified seismic assessment of multi-span masonry arch bridges. Bull Earthq Eng 2015. http://dx.doi.org/10.1007/s10518-015-9733-2.
[12] Zampieri P, Tecchio G, da Porto F, Modena C. Limit analysis of transverse seismic capacity of multi-span masonry arch bridges. Bull Earthq Eng 2015;13(5). http://dx.doi.org/10.1007/s10518-014-9664-3. 1557-152.
[13] Zampieri P, Zanini MA, Faleschini F. Influence of damage on the seismic failure analysis of masonry arches. Constr Build Mater 2016;119:343–55. http://dx.doi.org/10.1016/j.conbuildmat.2016.05.024.
[14] Da Porto F, Tecchio G, Zampieri P, Modena C, Prota A. Simplified seismic assessment of railway masonry arch bridges by limit analysis. Struct Infrastruct Eng 2015;11(4):415–42. http://dx.doi.org/10.1080/15732479.2015.1031141.
[15] Dimitri R, Tornabene F. A parametric investigation of the seismic capacity for masonry arches and portals of different shapes. Eng Fail Anal 2015;52:1–34.
[16] Cavicchi A, Gambarotta L. Collapse analysis of masonry bridges taking into account arch-fill interaction. Eng Struct 2005;27:605–15.
[17] Cavicchi A, Gambarotta L. Lower bond limit analysis of masonry bridges including arch-fill interaction. Eng Struct 2007;29:3002–14.
[18] Gago AS, Alfaiate J, Lamas A. The effect of the infill in arched structures: analytical and numerical modelling. Eng Struct 2011;33:1450–8. http://dx.doi.org/10.1016/j.engstruct.2010.12.037.
[19] Archie-M Masonry arch analysis software. (http://www.obvis.com/).

[20] Ring. Masonry Arch Bridge Analysis Software. (http://www.limitstate.com/ring).
[21] Brencich A, De Francesco U. Assessment of multispan masonry arch bridges. I: Simplified approach. J Bridge Eng 2004;9:582–90. http://dx.doi.org/10.1061/(ASCE)1084-0702(2004) 9:6(591).
[22] de Felice G, De Santis S. Experimental and numerical response of arch bridge historic masonry under eccentric loading. Int. J. Architect. Heritage 2010;4:115–37. http://dx.doi.org/10.1080/15583050903093886.
[23] De Santis S, de Felice G. Overview of railway masonry bridges with safety factor estimate. Int. J. Architect. Heritage 2014;8:452–74. http://dx.doi.org/10.1002/eqe.2416.
[24] Clemente P, Occhiuzzi A, Raithel A. Limit behaviour of stone arch bridges. J. Struct. Eng., ASCE 1995;121(7):1045–50.
[25] Clemente P, Saitta F. Analysis of no-tension material arch bridges with finite compression strength. J Struct Eng (United States)2017; 143(1), art. no. 04016145.
[26] Melbourne C, Gilbert M. Behaviour of multi-ring brickwork arch bridges. Struct Eng 1995;73:39–47.
[27] Modena C, Tecchio G, Pellegrino C, da Porto F, Dona M, Zampieri P, et al. Reinforced concrete and masonry arch bridges in seismic areas: typical deficiencies and retrofitting strategies. Struct Infrastruct Eng 2015;11(4):415–42. http://dx.doi.org/10.1080/15732479.2014.951859.
[28] Garmendia L, San-José JT, García D, Larrinaga P. Rehabilitation of masonry arches with compatible advanced composite material 2011;25(12):4374–85. http://dx.doi.org/10.1016/j.conbuildmat.2011.03.065.
[29] Giamundo V, Lignola GP, Maddaloni G, Balsamo A, Prota A, Manfredi G. Experimental investigation of the seismic performances of IMG reinforcement on curved masonry elements 2015;70: 53–63. http://dx.doi.org/10.1016/j.compositesb.2014.10.039.
[30] Marini A, Belleri A, Preti M, Riva P, Giuriani E. Lightweight extrados restraining elements for the anti-seismic retrofit of single leaf vaults. Eng Struct 2017;141:543–54.
[31] Anania L, D'Agata G. Limit analysis of vaulted structures strengthened by an innovative technology in applying CFRP. Constr Build Mater 2017;145:336–46.
[32] Alexakis H, Makris N. Limit equilibrium analysis and the minimum thickness of circular masonry arches to withstand lateral inertial loading. Arch Appl Mech 2014;84:757–72.
[33] Coccia S, Como M. Minimum thrust of rounded cross vaults. Int J Archit Herit 2015;9(4):468–84.
[34] Forgács T, Sarhosis V, Bagi K. Minimum thickness of semi-circular skewed masonry arches. Eng Struct 2017;140:317–36.
[35] Aita D, Barsotti R, Bennati S. Explicit solutions for depressed masonry arches loaded until collapse—Part I: a one-dimensional nonlinear elastic model. Meccanica 2017;52(4–5):989–1001.
[36] Aita D, Barsotti R, Bennati S. Explicit solutions for depressed masonry arches loaded until collapse—Part II: a solution method for statically indeterminate systems. Meccanica 2017;52(4–5):1093–106.
[37] Milani G, Lourenço PB. 3D non-linear behavior of masonry arch bridges. Comput Struct 2012;110–111:133–50. http://dx.doi.org/10.1016/j.compstruc.2012.07.008.
[38] Costa C, Ribeiro D, Jorge P, Silva R, Arêde A, Calçada R. Calibration of the numerical model of a stone masonry railway bridge based on experimentally identified modal parameters. Eng Struct 2016;123:354–71.
[39] Bergamo O, Campione G, Donadello S, Russo G. In-situ NDT testing procedure as an integral part of failure analysis of historical masonry arch bridges. Eng Fail Anal 57, 31–55.
[40] Bergamo O, Campione G, Cucchiara C, Russo G. Structural behavior of the old masonry bridge in the Gulf of Castellammare. Eng Fail Anal 2016;62:188–98.
[41] Fortunato A, Fabbrocino F, Angelillo M, Fraternali F. Limit analysis of masonry structures with free discontinuities. Meccanica 2017:1–10.
[42] Molins, C., Roca, P. Capacity of masonry arches and spatial frames. J Struct Eng 1998;124(6):653–63.
[43] Bernat-Maso E, Gil L, Marcé-Nogué J. The structural performance of arches made of few vossoirs with dry-joints. Struct Eng Mech 2012;44(6):775–99.
[44] O'Dwyer DW. Funicular analysis of masonry vaults. Comput Struct 1999;73:187–97.
[45] Block P, Ciblac T, Ochsendorf J. Real-time limit analysis of vaulted masonry buildings. Comput Struct 2006;84:1841–52.
[46] Block P, Ochsendorf J. Thrust network analysis: a new methodology for three-dimensional equilibrium. J Int Assoc Shell Spat Struct 2007;48(3):167–73.
[47] Makris N, Alexakis H. The effect of stereotomy on the shape of the thrust-line and the minimum thickness of semicircular masonry arches. Arch Appl Mech 2013;83:1511–33.
[48] Block P, Lachauer L. A three-dimensional funicular analysis of masonry vaults. Mech Res Commun 2014;56:53–60.
[49] Block P, Lachauer L. Three-dimensional equilibrium analysis of gothic masonry vaults. Int J Arch Heritage 2014;8:1–24.
[50] Marano G, Trentadue F, Petrone F. Optimal arch shape solution under static vertical loads. Acta Mech 2014;225:379–686.
[51] Cavalagli N, Gusella V, Severini L. The safety of masonry arches with uncertain geometry. Comput Struct 2017;(188):17–31.
[52] Moreira VN, Fernandes J, Matos JC, Oliveira DV. Reliability-based assessment of existing masonry arch railway bridges. Constr Build Mater 2016;115:544–54.
[53] Casas JR. Reliability-based assessment of masonry arch bridges. Constr Build Mater 2011;25:1621–31.
[54] Moreira VN, Matos JC, Oliveira DV. Probabilistic-based assessment of a masonry arch bridge considering inferential procedures. Eng Struct 2017;134:61–73. http://dx.doi.org/10.1016/j.engstruct.2016.11.067.
[55] Conde B, Ramos LF, Oliveira DV, Riveiro B, Solla M. Structural assessment of masonry arch bridges by combination of non-destructive testing techniques and three-dimensional numerical modelling: application to Vilanova bridge. Eng Struct 2017;148:621–38. http://dx.doi.org/10.1016/j.engstruct.2017.07.011.
[56] Zampieri P, Zanini MA, Faleschini F. Derivation of analytical seismic fragility functions for common masonry bridge types: methodology and application to real cases. Eng Fail Anal 2016;68:275–91. http://dx.doi.org/10.1016/j.engfailanal.2016.05.031.
[57] Zampieri P, Zanini MA, Faleschini F, Hofer L, Pellegrino C. Failure analysis of masonry arch bridges subject to local pier scour. Eng Fail Anal 2017;79:371–84. http://dx.doi.org/10.1016/j.engfailanal.2017.05.028.
[58] Como M. On the role played by Settlements in the statics of masonry structures. In: The conference on geotechnical engineering for the preservation of monuments and historic sites, Napoli, Italy, October, Balkema, Rotterdam; 1996. p 3–4.
[59] Ochsendorf JA. Collapse of masonry structures. Dissertation, Cambridge University Department of Engineering, Cambridge; 2002.
[60] Ochsendorf JA. The masonry arch on spreading supports. Struct Eng Inst Struct Eng Lond 2006;84(2):29–36.
[61] Coccia S, Di Carlo F, Rinaldi Z. Collapse displacements for a mechanism of spreading-induced supports in a masonry arch. Int J Adv Struct Eng 2015;7(3):307–20. http://dx.doi.org/10.1007/s40091-015-0101-x.
[62] Romano A, Ochsendorf JA. The mechanics of gothic masonry arches. Int J Archit Herit 2010;4(1):59–82.
[63] Heyman J. The stone skeleton. Int J Solids Struct 1966;2:249–79.
[64] Heyman J. The Masonry Arch, Ellis Horwood Ltd.; 1982.
[65] Drosopoulos GA, Stavroulakis GE, Massalas CV. Limit analysis of a single span masonry bridge with unilateral frictional contact interfaces. Eng Struct 2006;28(13):1864–73.